Kinetic and Fuel Property Effects on Forward Smoldering Combustion

S. V. LEACH, G. REIN, J. L. ELLZEY, and O. A. EZEKOYE
Department of Mechanical Engineering, University of Texas, Austin, TX 78712

and

J. L. TORERO
Department of Fire Protection Engineering, University of Maryland, College Park, MD USA

In this paper, we present the results from a one-dimensional transient model of forward smoldering. Fuel oxidation and pyrolysis reactions as well as a char oxidation reaction are included in the model. The solid energy, solid species, gas energy, oxygen species (bulk gas and surface), and overall mass conservation equations were discretized in space using finite-difference techniques and were solved using VODE, an ordinary differential equation integrator designed for stiff equations. Local thermal and chemical nonequilibrium are allowed in this model and transfer coefficients are derived from a Nusselt number correlation. A base case is chosen to represent experimental conditions reported in the literature. The effects of inlet gas velocity, kinetic frequency factors, inlet oxygen concentration, and fuel properties such as specific heat, density, conductivity, and pore diameter were studied using this model.

NOMENCLATURE

A	frequency factor
c	specific heat
D	diffusion coefficient
d	pore diameter
E_a	activation energy
f	exponent
g	exponent
hA'''	volumetric heat transfer coefficient
h_mA'''	volumetric mass transfer coefficient
k	conductivity
m	exponent
n	stoichiometric coefficient
R	gas constant
T	temperature
u	gas velocity
v	smolder velocity
V	diffusion gas velocity
x	coordinate
y	mass fraction

Greek Symbols

Δh	enthalpy of reaction
ϕ	porosity
ρ	density
ω	mass rate of production

Subscripts

a	ash
b	bulk gas
c	char
f	fuel
g	gas
i	inlet
o	oxidation
O_2	oxygen
p	pyrolysis
s	surface

INTRODUCTION

Smoldering is generally classified as either forward smolder in which the reaction zone propagates in the same direction as the oxidizer flow, or reverse smolder in which the reaction zone propagates opposing the oxidizer flow. Reverse smolder has been considered a more common fire initiation scenario, therefore it has been studied significantly. Ohlemiller provides two extensive reviews [1, 2] of the experimental and theoretical studies present in the literature. Reverse smolder is characterized by a steady propagation velocity and does not transition towards flaming [3, 4]. An increasing propagation velocity which eventually transitions to

*Corresponding author. E-mail: jellzey@mail.utexas.edu

0010-2180/00/$–see front matter
PII S0010-2180(99)00089-9

COMBUSTION AND FLAME 120:346–358 (2000)

Published by Elsevier Science Inc.

flaming [3, 5] is typical of forward smoldering. Thus, forward smoldering is a more dangerous, but less common fire scenario. Forward smoldering has received relatively little attention, although several notable experimental and theoretical studies can be found in the literature.

Ohlemiller and Lucca [3] experimentally compared the characteristics of forward and reverse smolder of cellulose. They noted qualitative and quantitative differences in the two smolder propagation modes. Reverse smolder quickly reaches a steady propagation rate determined mainly by heat transfer processes, whereas forward smolder propagation is unsteady and moves at a lower rate that appears limited by the stoichiometry of char oxidation. For forward smolder, two distinctive reactions were observed, a nonoxidative pyrolysis reaction and a char oxidation reaction.

Torero and Fernandez-Pello [5] conducted an experimental study of forward smolder of polyurethane foam. Air was used as an oxidizer and was forced in the direction of smolder propagation under conditions that approximate one-dimensional forward smolder propagation. Temperature history measurements at several locations throughout the foam sample were used to infer the characteristics of the smolder process and to calculate the smolder propagation velocity as a function of the air flow velocity. As the flow velocity was increased, there was a transition in the smolder characteristics from a smolder process that is characterized by the propagation of a single exothermic oxidation reaction to one characterized by the propagation of two reactions, an oxidative smolder reaction preceded by an endothermic pyrolysis reaction. Transition to flaming was observed in some experiments for air velocities larger than 15 mm/s.

The interpretation of Torero and Fernandez-Pello [5] of the forward smolder characteristics is somewhat different from that of Ohlemiller and Lucca [3] who interpret a thermal wave followed by a char oxidation reaction. Ohlemiller and Lucca [3] argue that since the oxidizer flows through the char, it has to be totally consumed for the reaction to propagate. Torero and Fernandez-Pello [5] observe the char not being totally consumed by the flowing oxidizer and offer as an explanation the possibility that char has a different reactivity than that of the virgin foam and requires different conditions of air supply or temperature for its oxidation. Although the geometry is slightly different, the results of Tse et al. [6] are in good agreement with the phenomenological explanations proposed by Torero and Fernandez-Pello [5].

A theoretical model of forward smolder was developed by Dosanjh et al. [7]. Two reaction zones were included: a nonoxidative pyrolysis reaction that decomposed the fuel into char followed by a char oxidation reaction. Buckmaster and Lozinski [8] developed a similar model providing a more elaborate description of the structure of the oxidation and pyrolysis fronts.

Schult et al. [9] employed asymptotic methods to find smolder wave solutions with two different structures, a reaction leading wave structure when the velocity of the combustion layer exceeds that of the heat transfer layer, and a reaction trailing wave structure obtained when the combustion layer is slower than the heat transfer layer. The reaction leading wave structure occurs when the incoming oxygen concentration is sufficiently high. The solutions obtained provide qualitative theoretical descriptions of the various experimental observations of forward smolder where the reaction trailing stoichiometric solutions correspond to the experimental observations of Ohlemiller and Lucca [3] and the reaction leading stoichiometric solutions correspond to the experimental observations of Torero and Fernandez-Pello [5].

In this paper, forward smoldering is examined using transient one-dimensional simulations. Our approach differs from most earlier models in that we assume neither thermal nor chemical equilibrium between the solid and gas phases. Only Ohlemiller [2] who presents independent energy equations for the gas and solid phase and Summerfield et al. [10] (for forward smolder) assume thermal nonequilibrium. Fatehi and Kaviani [11] incorporate some form of chemical nonequilibrium for reverse smolder.

We use our numerical model to simulate the experiments of Torero and Fernandez-Pello [5]. Fuel and char properties such as porosity, pore diameter, and fiber diameter were chosen to agree with the experimental values. The structure of the reaction front is compared to the

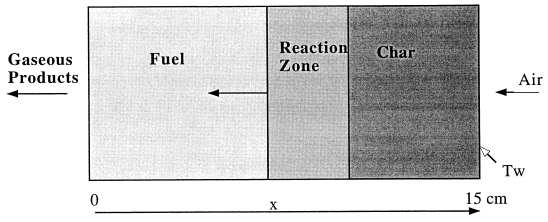

Fig. 1. Sketch of the forward smoldering configuration with forced air flow. The right side ($x = 15$ cm) is held at 600 K. Air (23% O_2 by mass) is forced through the right side at 0.53 cm/s.

observations of Torero and Fernandez-Pello. Then we examine the sensitivity of the results to the choice of kinetic constants and evaluate the effect of oxygen concentration and various fuel properties.

NUMERICAL MODEL

In this study, we solve the one-dimensional time-dependent conservation equations for the solid and the gas. The domain for these computations is shown in Fig. 1. The entire domain initially consists of unreacted fuel. Air flows in at the right boundary. Ignition is initiated by holding the right boundary at a specified temperature. The reaction zone in these simulations propagates from right to left.

Governing Equations

The following conservation equations for the solid and the gas are solved:

Solid energy equation:

$$\rho c \frac{\partial T}{\partial t} = \frac{\partial}{\partial x}\left(k_s \frac{\partial T}{\partial x} + \vec{q}_{rad}\right) - \omega_o \Delta h_o - \omega_p \Delta h_p - \omega_a \Delta h_a + hA'''(T_g - T) \quad (1)$$

Solid species equations:

$$\frac{\partial}{\partial t}(\rho y_c) = \omega_o n_{cl} + \omega_p n_{c2} - \omega_a \quad (2)$$

$$\frac{\partial}{\partial t}(\rho y_a) = n_{a3}\omega_a \quad (3)$$

Gas-phase energy:

$$\phi \rho_g c_{pg}\left(\frac{\partial T_g}{\partial t} + u\frac{\partial T_g}{\partial x}\right) = \phi k_g \frac{\partial^2 T_g}{\partial x^2} + hA'''(T - T_g) \quad (4)$$

Gas-phase continuity:

$$\frac{\partial}{\partial t}(\rho_g \phi) + \frac{\partial}{\partial x}(\rho_g \phi u) = \phi[\omega_p n_{g2} + \omega_o(n_{g1} - n_{o1}) + \omega_a(n_{g3} - n_{o3})] \quad (5)$$

Oxygen species in the bulk gas:

$$\frac{\partial}{\partial t}(\rho_g \phi_b y_{O_{2_b}}) + \frac{\partial}{\partial x}(\rho_g \phi_b u_b y_{O_{2_b}}) + \frac{\partial}{\partial x}(\rho_g \phi_b y_{O_{2_b}} V_{O_{2_b}}) = -h_m A'''(y_{O_{2_b}} - y_{O_{2_s}}) \quad (6)$$

Oxygen species at the surface:

$$\frac{\partial}{\partial t}(\rho_{g_s} \phi_s y_{O_{2_s}}) + \frac{\partial}{\partial x}(\rho_{g_s} \phi_s u_s y_{O_{2_s}}) + \frac{\partial}{\partial x}(\rho_{g_s} \phi_s y_{O_{2_s}} V_{O_{2_s}}) = -\omega_O n_{O1} - \omega_a n_{o3} + h_m A'''(y_{O_{2_b}} - y_{O_{2_s}}) \quad (7)$$

where all symbols are as defined in the Nomenclature.

Equations 6 and 7 account for the diffusion of oxygen at the surface of the solid. An obvious similarity exists between heat transport between the solid and gas and mass transfer between the solid and bulk gas. The chemical reactions occur at the surface of the fuel and depend on the amount of oxygen at this surface. To account for this bulk gas to surface diffusion process, the species equation can be rewritten in terms of oxygen in the bulk gas ($\phi_b y_{O_2 b}$), oxygen at the surface ($\phi_s y_{O_2 s}$), and a mass transfer coefficient (h_m). In these equations, the subscript b refers to the bulk gas, s refers to the surface, and $\phi_b + \phi_s = \phi$ where ϕ is the volume fraction of gas (or the porosity of the material). In our case, $\phi_s \ll \phi_b$ and so the contribution of the terms on the left-hand side of Eq. 7 is negligible. We can assume that u_s, the gas velocity at the surface, is zero so that the second term in the oxygen

species equation at the surface is zero. In addition, the third term on the left-hand side of Eq. 7 is usually negligible but is included for completeness.

In addition to the above equations, V_{O_2}, the diffusion velocity of oxygen, is calculated from

$$V_{O_2} = -D_{O_2 m} \frac{\partial y_{O_2}}{\partial x} \tag{8}$$

where y_{O_2} is the mass fraction of oxygen and m denotes the mixture.

Kinetics

A three-step reaction model that allows for char formation and oxidation given by Rogers and Ohlemiller [12] is as follows:

Exothermic thermal oxidation:

$$1g(\text{fuel}) + n_{O1}\text{O}_2 \rightarrow n_{c1}(\text{char}) + n_{g1}(\text{gases}) \tag{9a}$$

Endothermic pyrolysis:

$$1g(fuel) \rightarrow n_{c2}(char) + n_{g2}(gases) \tag{9b}$$

Exothermic char oxidation:

$$1g(char) + n_{O3}O_2 \rightarrow n_{a3}(ash) + n_{g3}(gases) \tag{9c}$$

The mass rates of production are similar to those given by Kashiwagi and Nambu [13] and are of the following form:

Thermal oxidation:

$$\omega_o = (1 - y_c - y_a)^f \rho_f A_o (y_{o_2})^m e^{-E_{a_o}/RT} \tag{10a}$$

Pyrolysis:

$$\omega_p = (1 - y_c - y_a)^g \rho_f A_p e^{-E_{a_p}/RT} \tag{10b}$$

Char oxidation:

$$\omega_a = y_c \rho_c A_a (y_{O_2})^h e^{-E_{a_a}/RT} \tag{10c}$$

where y_c is the char fraction, y_{O_2} is the mass fraction of oxygen, y_a is the ash fraction, and the other symbols are defined in the Nomenclature.

Heat and Mass Transfer Coefficients

The volumetric transfer coefficients are modeled as functions of Reynolds and Prandtl numbers. Wakao and Kaguei [14] proposed the following correlation for the internal coefficient of heat transfer between a packed bed of spheres and the fluid forced through it:

$$Nu = \frac{h d_p}{k_g} = 2 + 1.1 Re^{0.6} Pr^{1/3} \tag{11}$$

where h is the interstitial heat transfer coefficient (per surface area of a particle); d_p is the diameter of spherical particle which is the fiber diameter in our case; k_g is the gas thermal conductivity; $Re = u\phi d_p/\nu$, and $Pr = \nu/\alpha$. For a packed bed of cylinders, $Nu_{\text{cylinder}} = 0.79Nu$ (15). The specific interfacial gas solid surface is

$$A''' = \frac{4(1 - \phi)}{d} \tag{12}$$

where d is the pore diameter. Several heat transfer correlations were considered for use in this model: packed bed of spheres, packed bed of cylinders, and cylinders in cross-flow. In all cases, these correlations predicted high heat transfer coefficients which resulted in solid and gas temperatures which were within 5 K.

Incroprera and Dewitt [15] present a heat and mass transfer analogy so that the ratio of the heat transfer to mass transfer coefficients

$$\frac{h}{h_m} = \rho_g c_p Le^{(1-n)}$$

where $Le = \alpha/D$. For most applications it is reasonable to assume a value of $n = 1/3$.

Property Definitions

We use the char mass fraction y_c and the ash mass fraction as y_a to define the solid properties. In our simulations, the oxidation of char into ash resulted in high temperatures which would most likely promote flaming. Because our model did not include gas-phase reactions typical of flaming combustion, all of the simulations were terminated once the char oxidation reaction was initiated. Therefore, these results do not include cases in which ash is a significant component of the material. For simplicity then, we assume that the properties for char and ash are the same. Radiation heat transfer is modeled in the optically thick limit [22]. For this limit, the radiative flux vector is proportional to the temperature gradient. The constant of pro-

portionality may be thought of as a "radiative conductivity". The total thermal conductivity is given as

$$k = k_{con} + k_{rad} \tag{13}$$

$$k_{con} = (y_c + y_a)k_c + (1 - (y_c + y_a))k_f \tag{14}$$

$$k_{rad} = 16\sigma d T^3/3 \tag{15}$$

and σ is the Stefan-Boltzmann constant, T is the solid temperature, and d is the pore diameter.

As the smolder wave propagates, the solid fuel reacts and becomes char which has different properties than the unreacted fuel. The solid properties (e.g., density, conductivity, pore diameter) at any computational cell are calculated based on a mass-weighted average of the pure fuel and char properties.

Boundary and Initial Conditions

The computational domain is shown in Fig. 1. The right boundary is at a specified temperature, T_w. Air flows through the right boundary into the fuel bed. The smolder front propagates from right to left. At the left boundary $x = 0$, the hot gases exit and the gradients are assumed to be zero:

$$\frac{\partial T}{\partial x} = 0, \frac{\partial T_g}{\partial x} = 0, \frac{\partial y_{O_2}}{\partial x} = 0 \tag{16}$$

At the right boundary $x = l$, the wall is held at a fixed temperature and the inlet gas temperature, composition, and velocity are specified:

$$T = T_W, T_g = T_{gin}, y_{O_2} = y_{O_2 in}, u = u_{in} \tag{17}$$

At $t = 0$, the entire fuel bed is unreacted, the temperatures of the fuel and gas are constant, and the composition of the gas is constant

$$T = T_{in}, T_g = T_{g_{in}}, y_{O_2} = y_{O_{2in}}, y_c = 0 \tag{18}$$

The smolder wave is initiated by bringing the solid temperature to 600 K at the boundary and maintaining that temperature until the smolder wave begins to propagate.

Solution Method

The solid energy, gas energy, char species, ash species, and oxygen species (bulk and surface), and continuity equations are discretized in space using finite-difference techniques. For this problem, the package DVODE [16] is used. DVODE is an ordinary differential equation integrator designed for stiff equations and is frequently used in applications involving chemical kinetics. Solid temperature, char fraction, ash fraction, oxygen concentration at the surface, oxygen concentration in the bulk gas, and gas temperature are all solved using the above techniques. Gas velocity is solved directly using the overall continuity equation.

In this model, it is assumed that the pressure drop across the pile was negligible. In order to discover when this assumption is valid, the conservation of momentum equation was nondimensionalized. It was found that for high porosity, the momentum equation (i.e., the Darcy law) becomes trivial. In all of our cases, the porosity was 0.98.

Calculations were performed for 50 to 400 grid points for the base case to ensure grid independence of the results. All of the computations discussed in this paper were performed on a uniform grid of 400 points. Time step selection is controlled by DVODE. We tested several different error criteria (relative tolerances) to ensure that time stepping is accurate.

RESULTS

In this section, the results from the one-dimensional simulations of forward smoldering are presented. The geometry is shown in Fig. 1. We first simulate a case similar to that studied experimentally by Torero and Fernandez-Pello [5]. Then the importance of various parameters on the smoldering process is examined. In the base case described below, we include the effects of chemistry, transport, and convective and radiative heat transfer.

General Smoldering Characteristics

We chose property values to represent the smoldering of a porous bed of polyurethane foam as our base case in order to compare to experimental measurements by Torero and Fernandez-Pello [5]. The material properties are given in Table 1. Because kinetic parameters for

TABLE 1

Properties

Property	Value	Reference
Δh_O	−5700 J/g	Kashiwagi and Nambu [13]
Δh_p	570 J/g	Kashiwagi and Nambu [13]
Δh_a	−25,000 J/g	Kashiwagi and Nambu [13]
n_{O1}	0.41	Kashiwagi and Nambu [13]
n_{c1}	0.21	Kashiwagi and Nambu [13]
n_{c2}	0.24	Kashiwagi and Nambu [13]
n_{O3}	1.65	Kashiwagi and Nambu [13]
n_{a3}	0.03	Kashiwagi and Nambu [13]
A_o	5.69×10^{11} L/s	estimated
E_{ao}/R	19,245 K	Kashiwagi and Nambu [13]
f	1.3	Kashiwagi and Nambu [13]
m	0.5	Kashiwagi and Nambu [13]
A_p	2×10^{17} L/s	Kashiwagi and Nambu [13]
E_{ap}/R	26,500 K	Kashiwagi and Nambu [13]
g	1.8	Kashiwagi and Nambu [13]
A_a	5×10^{8} L/s	estimated
E_{aa}/R	19,244 K	Kashiwagi and Nambu [13]
h	0.78	Kashiwagi and Nambu [13]
k_c	4.2×10^{-2} W/mK	Di Blasi [20]
k_f	6.3×10^{-2} W/mK	Di Blasi [20]
d_f	0.00005 m	Fatehi and Kaviany [21]
d_c	0.0013 m	estimated
d_{fiber}	0.00001 m	
ρ_c	10 kg/m^3	estimated
ρ_f	26.5 kg/m^3	Torero et al. [4]
c_c	1.1 kJ/(kgK)	Di Blasi [20]
c_f	1.7 kJ/(kgK)	Torero et al. [4]
k_g	2.58×10^{-2} W/mK	Di Blasi [20]
ϕ_f	0.98	Torero et al. [4]
ϕ_c	0.98	estimated
D_{O2m}	4.53×10^{-5} m^2/s	Torero et al. [4]
T_W	600 K	
T_{gin}	300 K	
y_{O2in}	0.23	
u_{in}	0.0053 m/s	Torero et al. [4]

polyurethane foam were unavailable, data similar to those for cellulosic paper [13] were used. The activation energies and values of heat of reaction for all three reactions, as well as the preexponential factor for the pyrolysis reaction are those given by Kashiwagi and Nambu [13], but the preexponential factors of the fuel and char oxidation reactions were estimated to match experiments at a specific inlet gas velocity (0.53 cm/s) and inlet oxygen concentration (0.23) and then held at these values for all other cases studied. The kinetic constants are different from those used for the fuel oxidative reaction in Leach et al. [17, 18] because in those earlier computations we calibrated the kinetics with a low inlet gas velocity. Since then we discovered that smolder propagation with low inlet gas velocities is controlled by diffusive processes rather than by chemical kinetics. At higher inlet gas velocities, the propagation is dominated by kinetics. So in the computations presented here, the oxidative frequency factor was calibrated with the inlet gas velocity of 0.53 cm/s.

In Fig. 2, the profiles of solid temperature, oxygen mass fraction, and net heat release are presented. Each line represents a different time step and results are plotted in approximately 50-second increments. Initially, the solid is at 300 K. Air (23% oxygen by mass) is forced through the right boundary at 0.53 cm/s. Ignition is modeled by increasing the temperature at the right boundary exponentially from 300 K to 600 K over 500 seconds. The smolder wave propagates from right to left in this plot.

At 1065 s, the smolder wave is located at approximately $x = 14.5$ cm. The peak temperature for all later times is ~650 K. In a frame of reference attached to the smolder front, the fuel and oxidizer enter the reaction zone from opposite sides. At later times, the fuel has been preheated relative to earlier times and more oxygen is consumed at each successive time step (Fig. 2).

The net peak heat release remains relatively constant after about 1216 s. The negative region is due to the endothermic pyrolytic reaction which becomes more important as the smolder wave propagates through the fuel bed due to the increased temperature of the unreacted fuel. The pyrolytic front preceeds the oxidative front and results in the inflection point in the temperature profiles (Fig. 2).

In Fig. 3, the heat releases for the three reactions (exothermic fuel oxidation, endothermic fuel pyrolysis, and exothermic char oxidation) are shown. The magnitudes of the fuel oxidation and pyrolysis heat releases are comparable, but the char oxidation heat release is small in comparison. In later time steps the endothermic pyrolysis reaction becomes even more important and an endothermic pyrolysis front is followed by an exothermic oxidation front as observed in the net heat release profiles. This phenomenon has also been observed experimentally by Torero and Fernandez-Pello

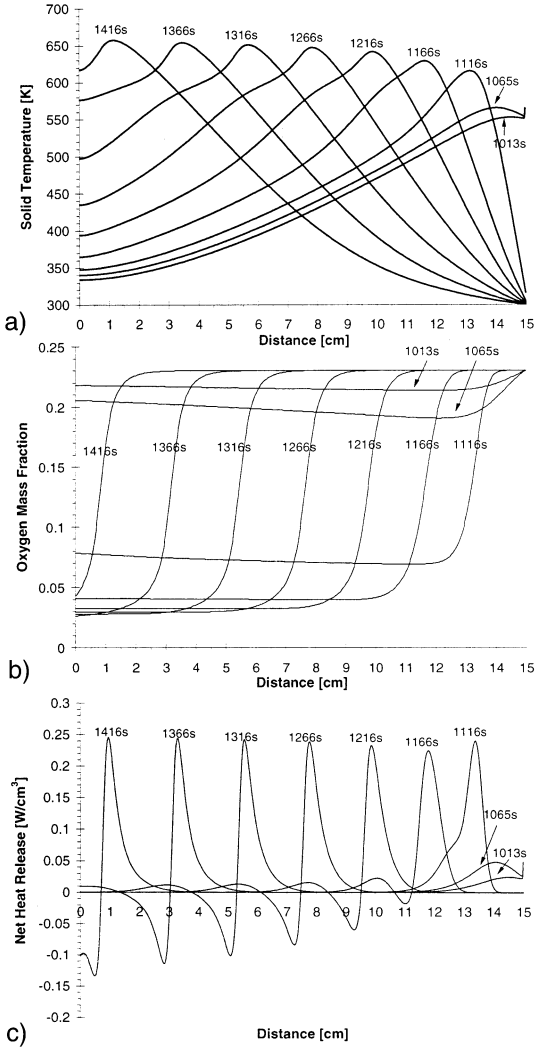

Fig. 2. (a) Solid temperature, (b) oxygen mass fraction, and (c) net heat release vs. distance for the base case of forward smoldering. The solid temperature is brought to 600 K at $x = 15$ cm until smolder wave begins to propagate and is insulated at $x = 0$ cm. Air at 300 K is forced at 0.53 cm/s at $x = 15$ cm.

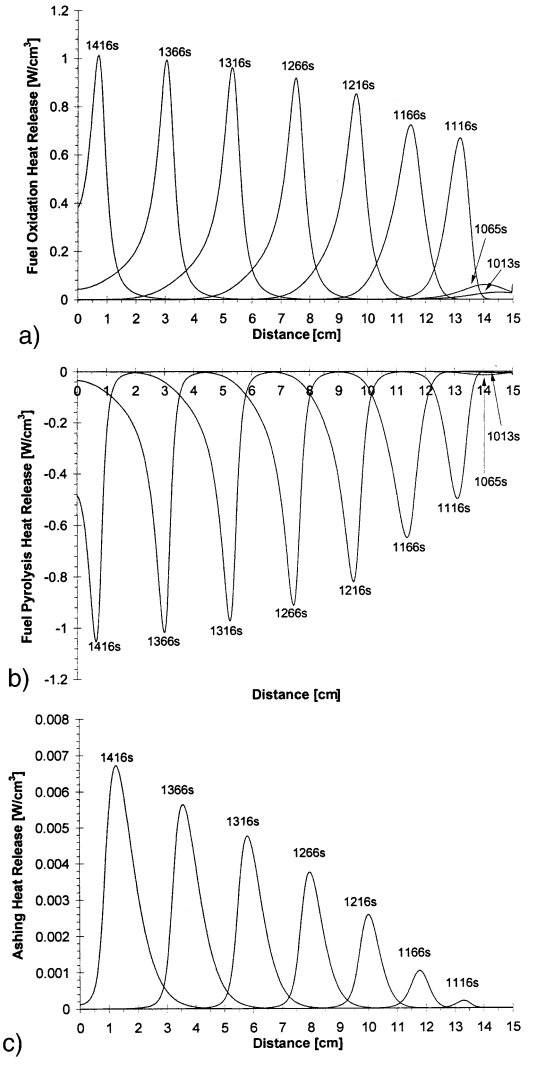

Fig. 3. (a) Fuel oxidation heat release, (b) fuel pyrolysis heat sink, and (c) char oxidation heat release vs. distance for the base case of forward smoldering.

[5]. The increasing effect of the endothermic reaction at later times is due to the decreased oxygen. As long as there is sufficient temperature and oxygen present, the fuel oxidation reaction can proceed. When there is limited oxygen, the endothermic pyrolysis reaction becomes more dominant.

The smolder wave velocity is measured at the oxidative front after the wave has propagated away from the boundary. This is the region identified as zone II in Torero and Fernandez-Pello [5]. We determined an average smolder velocity of 0.45 cm/s for this case.

The gas velocity through the solid material is shown in Fig. 4. The air velocity into the fuel at $x = 15$ cm is specified as 0.53 cm/s. As the air flows through the solid (from right to left), it is heated by convective heat transfer from the solid. The gas density decreases resulting in an increased velocity. Gasification in the reaction zone also causes the gas velocity to increase. The increase in gas velocity is more significant at later times due to the higher temperatures.

Figure 5 shows temperature vs. time from

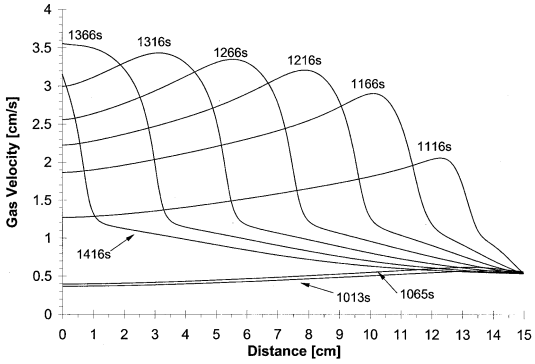

Fig. 4. Gas velocity vs. distance plotted for the base case of forward smoldering. Air at 300 K is forced at 0.53 cm/s at $x = 15$ cm.

ignition for various distances from ignition. This was plotted in order to compare with the experiments of Torero and Fernandez-Pello [5] whose results were presented this way. Each line represents a different axial location along the sample and the distance from the ignition location is indicated for each line. The data in Fig. 5 are for the same simulation as in Figs. 2, 3, and 4. The temperature profiles are the result of the complex interplay of the heat transfer mechanisms and the kinetics. For example, at 6 cm, the temperature increases from 1000 seconds to ~1225 seconds due to the heat transfer (i.e., conduction, convection, and radiation) of heat away from the reaction zone. There is no significant reaction taking place during this time. At ~1225 seconds, the endothermic pyrolytic front begins to pass the measurement location and a decrease in the slope of the temperature profile

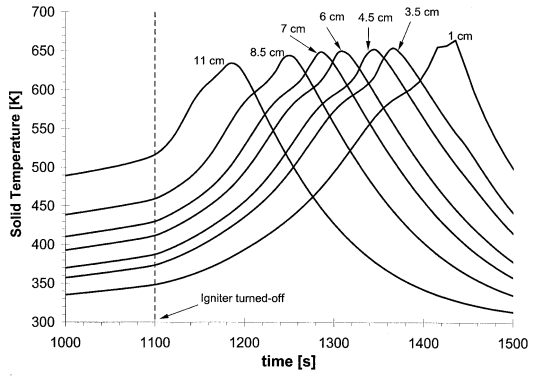

Fig. 5. Temperature histories at several locations along the foam sample. The inlet gas velocity is 0.53 cm/s and oxygen concentration is 0.23.

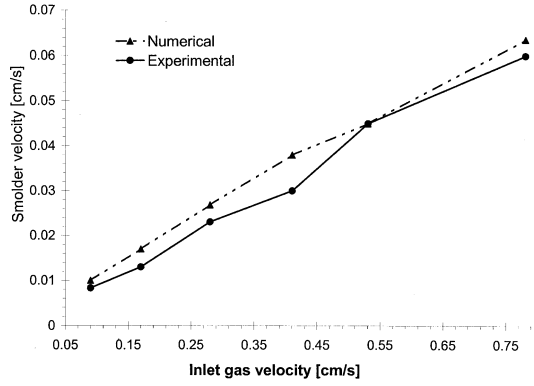

Fig. 6. Smolder velocity vs. inlet gas velocity for an oxygen concentration of 0.23. Experimental results are from Torero and Fernandez-Pello [5].

is observed. At ~1275 seconds, the exothermic oxidative front passes and the temperature increases rapidly. These qualitative features agree well with the experimental interpretation of Torero and Fernandez-Pello [5] and also with the experimental explanations of Tse et al. [6].

Effect of Inlet Gas Velocity and Comparison to Experimental Measurements

We examined the effect of inlet gas velocity on the smoldering of polyurethane foam. All of the parameters for the base case (Table 1) were used and the inlet gas velocity was varied from 0.09 cm/s to 0.78 cm/s. In Fig. 6, the calculated and measured smoldering velocity as a function of inlet gas velocity is shown. As noted above, the frequency factor for the oxidative reaction was calibrated at an inlet velocity of 0.53 cm/s but was not changed for the other cases. The computational results agree very well with the experimental measurements of Torero and Fernandez-Pello [5]. Both show a roughly linear increase in smolder velocity with inlet gas velocity.

Effects of Kinetic Frequency Factors

We studied the sensitivity of the smoldering characteristics to the frequency factor for the case where the inlet gas velocity is 0.53 cm/s. We varied the oxidative, the pyrolysis, or the char reaction frequency factor while holding the other two constant. These results are summarized in Table 2.

TABLE 2

Effect of Frequency Factors on Smolder Velocity

Case	A_O (s^{-1})	A_p (s^{-1})	A_a (s^{-1})	v (cm/s)	Characteristics
1a	1.00×10^{11}	2.00×10^{17}	5.00×10^{8}	0	Does not ignite
1b	3.50×10^{11}	2.00×10^{17}	5.00×10^{8}	0.032	Requires ~1500 s for smolder front to start propagating
1c	5.69×10^{11}	2.00×10^{17}	5.00×10^{8}	0.045	Base case: Requires ~1100 s for smolder front to start propagating
1d	8.00×10^{11}	2.00×10^{17}	5.00×10^{8}	0.061	
1e	2.00×10^{12}	2.00×10^{17}	5.00×10^{8}	0.1[a]	Ashing occurs when the smolder front is roughly in the center of the bed
2a	5.69×10^{11}	1.00×10^{10}	5.00×10^{8}	0	Cannot simulate the propagation because heat release is too high
2b	5.69×10^{11}	5.00×10^{16}	5.00×10^{8}	0.05[a]	Cannot simulate the propagation because heat release is too high
2c	5.69×10^{11}	1.00×10^{17}	5.00×10^{8}	0.07	Ashing occurs when smolder propagates through entire length
2d	5.69×10^{11}	5.00×10^{17}	5.00×10^{8}	0.022	Peak temperature is lower (590 K) and half of the fuel is left unburned
2e	5.69×10^{11}	1.00×10^{18}	5.00×10^{8}	—	Not self-sustaining unless fixed temperature boundary is maintained
3a	5.69×10^{11}	2.00×10^{17}	1.00×10^{8}	0.045	
3b	5.69×10^{11}	2.00×10^{17}	8.00×10^{8}	0.045	
3c	5.69×10^{11}	2.00×10^{17}	2.00×10^{9}	0.046	Ashing occurs after smolder front propagates through entire bed

[a] In these cases, the smolder velocity was measured immediately before the ashing started.

In case 1 (Table 2), the fuel oxidative frequency factor was varied from 1×10^{11} s^{-1} to 2×10^{12} s^{-1} while the fuel pyrolysis and char oxidation frequency factors were fixed at 2×10^{17} s^{-1} and 5×10^{8} s^{-1} respectively. Case 1c is the base case discussed above. We found that at the lowest frequency factor (case 1a), the smolder front failed to propagate and the smoldering process was kinetically limited. As the fuel oxidative frequency factor was further increased to 3.5×10^{11} s^{-1}, after about 1500 s, the smolder front began to propagate. Greater increases in the fuel oxidative frequency factor (cases 1c–e) resulted in less time required for ignition and faster smolder velocities [19].

In cases 2a–e, the fuel pyrolysis frequency factor was varied from 1.0×10^{10} to 1.0×10^{18} s^{-1} while the fuel oxidation frequency factor was held at 5.69×10^{17} s^{-1} and the char oxidation frequency factor was held at 5×10^{8} s^{-1}. When the pyrolysis frequency factor was low (case 2a and 2b), the temperature rise in the fuel occurred very rapidly because there was insufficient extraction of heat by the endothermic reaction and we could not successfully simulate the propagation. At a pyrolysis frequency factor of 1×10^{17} s^{-1} (case 2c), the ashing reaction occurred after the smolder front propagated throughout the entire sample. As the pyrolysis frequency factor is increased beyond the base case value of 2.0×10^{17} s^{-1} (case 2d) the peak temperature is lower and about half of the fuel is left unreacted. At still higher values, the smolder front cannot be sustained unless the temperature at the inlet boundary is held constant at 600 K. In contrast to the fuel oxidative reaction rate, the pyrolysis rate affects the smolder velocity over all values considered and can promote extinction. This is reasonable considering that pyrolysis only requires unreacted fuel to proceed.

Four char oxidation frequency factors were considered, 1×10^{8} s^{-1} (case 3a), 5×10^{8} s^{-1} (case 1c), 8×10^{8} s^{-1} (case 3b), and 2×10^{9} s^{-1} (case 3c). Cases 3a and 3b resulted in similar smolder velocities as the base case which is reasonable since the ashing reaction is not very important at these conditions. For the highest value of the char oxidation frequency factor (case 3c), ashing occurs after the smolder front

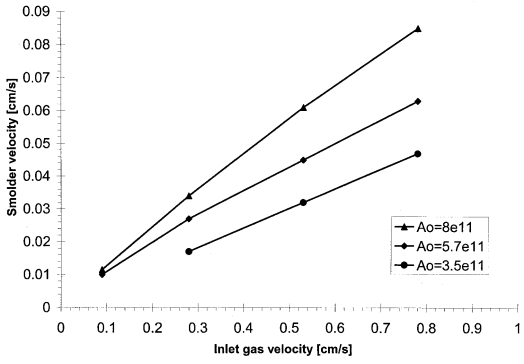

Fig. 7. Smolder velocity vs. inlet gas velocity for an oxygen concentration of 0.235 and different oxidation frequency factors. Experimental results are from Torero and Fernandez-Pello [5].

has propagated through the entire length of the fuel bed.

In the initial simulations, the kinetic constants were determined such that the smolder velocity at a low inlet gas velocity (0.53 cm/s) matched the experimental value. In our earlier studies of smoldering, it appeared that smoldering was oxygen limited at low inlet velocities and kinetically limited at higher velocities. Figure 7 shows the effect of the fuel oxidative frequency factor on smolder velocities over a range of inlet gas velocities. Three different oxidative frequency factors were used (3.5×10^{11}, 5.7×10^{11}, 8×10^{11} s^{-1}). The lowest inlet velocity of 0.1 cm/s did not result in a stable smolder wave for the frequency factor of 3.5×10^{11} s^{-1}. At lower inlet gas velocities, increasing the oxidative frequency factor had little effect on the smolder velocity, because the process was oxygen limited. As suspected, we observed that increasing the oxidative frequency factor resulted in higher smolder velocities for the higher inlet gas velocities, because the process was kinetically limited. These results indicate that although the same chemistry is driving the reactions over all conditions, the sensitivity of the smolder velocity to the selection of the kinetic constants varies according to whether the process is oxygen or kinetically limited.

Effect of Oxygen Concentration

The availability of oxygen to the smolder front is determined not only by the gas inlet velocity but also by the concentration of oxygen in the gas stream. We examined the effect of oxygen concentration on the base case by holding the gas

TABLE 3

Effect of Oxygen Concentration on Smolder Velocity

Case	y_{ox}	v (cm/s)	Characteristics
4a	0.05	0.022	Requires ~1500 s for smolder front to begin propagating. Peak temperature is 590 K (65 K lower than the base case) and peak heat release is 95% lower. 70% of the mass of the fuel is left unburned all over the sample.
4b	0.1	0.027	Requires ~1250 s for smolder front to begin propagating. Peak temperature is 610 K (45 K lower than the base case) and peak heat release is 80% lower. 30% of the mass of the fuel is left unburned all over the sample.
4c	0.23	0.045	Base case: Requires ~1100 s for smolder front to begin propagating. Peak temperature is 655 K. Less than 3% of the mass of the fuel is left unburned.
4d	0.3	0.057	Requires ~1050 s for smolder front to begin propagating. Peak temperature is 665 K (10 K higher than the base case) and peak heat release is 50% higher. No fuel is left unburned.
4e	0.4	—	Requires ~1050 s for smolder front to begin propagating. Ashing takes place at the middle.

TABLE 4

Effect of Fuel Properties on Smolder Velocity

Case	Property	Reference	v (cm/s)	Characteristics
5a	k = 0.047 W/mK	Torero et al. [4], polyurethane foam	0.045	Requires ~1100 s for smolder front to begin propagating.
5b	k = 0.063 W/mK	Di Blasi [20]	0.045	Base case. Requires ~1100 s for smolder front to begin propagating. Peak temperature is ~655 K.
5c	k = 0.113 W/mK	Kung [23], wood	0.045	Requires ~1100 s for front to begin propagating. Peak temperature is ~650 K and peak heat release is 5% lower than base case.
6a	ρ = 1.24 kg/m^3	Dosanjh et al. [24], alpha-cellulose	0.05	Requires ~1050 s for front to begin propagating. Peak temperature is around 675 K and peak heat release is 30% lower than base case. Ashing occurs at the end.
6b	ρ = 26.5 kg/m^3	Torero et al. [4], polyurethane foam	0.045	Base case
6c	ρ = 0.1 kg/m^3		0.009	Smolder front is not sustained unless boundary is maintained at the fixed temperature. Peak temperature is around 615 K and peak heat release is 50% higher than base case.
6d	ρ = 0.15 kg/m^3		0.005	Smolder front is not sustained unless boundary is maintained at the fixed temperature. Peak temperature is ~590 K.
7a	c_p = 0.84 kJ/kgK	Dosanjh et al. [24], alpha cellulose	0.06	Requires ~950 s for smolder front to begin propagating. Peak temperature is ~665 K.
7b	c_p = 1.7 kJ/kgK	Torero et al. [4], polyurethane foam	0.045	Base case
7c	c_p = 2.5 kJ/kgK	Kung [23], wood	0.031	Requires ~1250 s for smolder front to begin propagating. Peak temperature is ~645 K and peak heat release is 10% lower than base case. 7% of the mass of the fuel is left unburned.

velocity fixed at 0.53 cm/s but varying the oxygen concentration. All other values are those for the base case described earlier. These results are summarized in Table 3. At an inlet oxygen concentration of 0.05, about 70% of the fuel is left unreacted and the peak temperature is ~65 K lower than in the base case. When the inlet oxygen concentration is 0.01, about 30% of the fuel is unreacted. For the base case of an oxygen concentration of 0.23, almost all of the fuel is reacted as the smolder wave propagates through the fuel bed. At higher oxygen concentrations (0.3), the peak heat release and the smolder velocity are substantially higher than in the base case. At an oxygen concentration of 0.4, we observe that ashing takes place in the middle of the fuel bed.

Effect of Fuel Conductivity, Specific Heat, and Density

Fuel properties vary significantly among the different smoldering materials. In addition, measurements of a single material property may vary widely. To determine the sensitivity of our results to property values, we varied the conductivity, specific heat, and density of the fuel. These results are summarized in Table 4.

Three conductivities of fuel were considered (cases 5a–c). These values were selected from the literature for various materials as indicated in Table 4. Although we varied the conductivity by a factor of 2.4 from 0.047 W/mK to 0.113 W/mK, the smolder velocity remained constant at 0.45 cm/s. It appears that the other heat

TABLE 5

Effect of Pore Diameter on Smolder Velocity With and Without Radiation

Pore Diameter (cm)			v (cm/s)		
Fuel	Char	Reference	With radiation	Without radiation	Characteristics
0.005	0.005		0.045	0.045	Very similar profiles
0.005	0.13	Torero et al. [4]	0.045	0.045	Base case: Without radiation, heat release has higher peaks (15%) without radiation and temperature profiles are narrower
0.13	0.13		0.050	0.049	Without radiation, heat release has higher peaks (20%), temperature profiles are thinner narrower, and it takes 300 s longer time for ignition to occur
0.64	0.64				Temperature profiles are broader

transfer modes were more effective than conduction in preheating the fuel.

We varied the fuel density from 0.0124 kg/m^3 to 0.15 kg/m^3 (cases 6a–d). These densities represent the actual sample density including the effect of the high porosity ($\phi = 0.98$) as opposed to the actual material density. Increasing the density by almost a factor of 10 from 0.0124 kg/m^3 to 0.15 kg/m^3 decreased the smolder velocity by a factor of 10.

We varied the specific heat from 0.84 to 2.5 kJ/kgK (cases 7a–c). Some of these values were obtained from the literature for different materials as shown in Table 4. Changing the specific heat by a factor of 3 from 0.84 kJ/kgK to 2.5 kJ/kgK decreased the smolder velocity by a factor of 2 from 0.06 cm/s to 0.031 cm/s. These simulations indicate that density has a much greater effect on smolder velocity than conductivity and a somewhat greater effect than specific heat.

Effect of Pore Diameter

The pore diameter affects both convective and radiative heat transfer. Increasing the pore diameter decreases the volumetric heat transfer coefficient by decreasing the area to volume ratio and increases the radiative conductivity. In order to determine the effects of pore diameter, simulations were conducted for different values of fuel and char pore diameters with and without radiation. These results are summarized in Table 5. When the fuel and char pore diameters are small (0.005 cm), radiation is not important and the smolder velocity is the same. The temperature profiles with and without radiation are also very similar. When the fuel pore diameter is small (0.005 cm) and the char diameter is large (0.13) as with the material used by Torero and Fernandez-Pello [5], the smolder velocity is the same with and without radiation but the temperature profiles are more spread out when radiation is included. The peak heat release is about 15% higher without radiation. When the fuel and char pore diameters are both 0.13 cm, the smolder velocity is higher than in the other cases. Radiation, however, does not make a difference suggesting that the reduced convective heat transfer from the solid to the gas promotes higher solid temperatures and faster smolder velocities. It also was more difficult to ignite the case without radiation. When the pore diameters are very large (0.64 cm), the temperature profiles are quite spread out when radiation is included and it is difficult to discern the smolder front from these profiles.

SUMMARY AND CONCLUSIONS

In this paper, results of one-dimensional transient simulations of forward smoldering were presented. Fuel oxidation and pyrolysis as well as a char oxidation reaction were included in this model. A base case was chosen to represent a case experimentally studied by Torero and Fernandez-Pello [5]. The numerical model confirms their interpretations of the experimental results that an endothermic pyrolysis front is followed by an exothermic oxidative front, and after some time char oxidation occurs. The

effects of the kinetic frequency factors were also investigated giving a better estimate on the range of these kinetic parameters. A comparison of the effects of fuel conductivity, density, specific heat, and pore diameter indicated that fuel density is the most important and fuel conductivity is the least important factor in determining smolder velocity. The effect of inlet gas velocity was examined and good agreement was shown between the numerical simulations and experiments. It was also shown that at low gas velocities, the smolder process is oxygen limited and the oxidation frequency factor had little effect on the smolder velocity. However, at higher inlet gas velocities, the smolder process becomes kinetically limited and the smolder velocity is therefore highly dependent on the fuel oxidative frequency factor.

This work was sponsored by the Applied Research Laboratories at the University of Texas at Austin through the Office of Naval Research.

REFERENCES

1. Ohlemiller, T. J., *The SFPE Handbook of Fire Protection Engineering*, 3rd ed., 1995, pp. 2.171–2.179.
2. Ohlemiller, T. J., *Prog. Energy Combust. Sci*. 65:277–310 (1986).
3. Ohlemiller, T. J., and Lucca D. A., *Combust. Flame* 54:131–147 (1983).
4. Torero, J. L., Fernandez-Pello, A. C., and Kitano, M., *Combust. Sci. Technol*. 91:95–117 (1993).
5. Torero, J. L., and Fernandez-Pello, A. C., *Combust. Flame* 106:89–109 (1996).
6. Tse, S. D., Fernandez-Pello, A. C., and Miyasaka, K., *Twenty-Sixth Symposium (International) on Combustion*, The Combustion Institute, 1996, Vol. 1, pp. 1505–1513.
7. Dosanjh, S. S., Pagni, P. J., and Fernandez-Pello, *Proceedings of the 1987 ASME/JSME Thermal Engineering Joint Conference*, 1987, pp. 165–173.
8. Buckmaster, J., and Lozinski, D., *Combust. Flame* 104:300–310 (1996).
9. Schult, D. A., Matkowsky, B. J., Volpert, V. A., and Fernandez-Pello, A., *Combust. Flame* 104:1–26 (1996).
10. Summerfield, M., Ohlemiller, T. J., and Sandusky, H. W., *Combust. Flame* 33:263–279 (1978).
11. Fatehi, M., and Kaviany, M., *Combust. Flame* 99:1–17 (1994).
12. Rogers, F. E., and Ohlemiller, T. J., *Combust. Sci. Technol*. 76:129–137 (1980).
13. Kashiwagi, T., and Nambu, H. *Combust. Flame* 88: 345–368 (1992).
14. Wakao, N., and Kaguei, S., *Heat and Mass Transfer in Packed Beds*, Gordon and Breach, New York, 1982.
15. Incroprera, F. P., and Dewitt, D. P., *Fundamentals of Heat and Mass Transfer*, 3rd ed., John Wiley, 1990, p. 356.
16. Brown, P. N., Byrne, G. D., and Hindmarsh, A. C., *SIAM J. Sci. Stat. Comput*. 10:1038–1051 (1989).
17. Leach, S. V., Ellzey, J. L., and Ezekoye, O. A., *Twenty-Seventh Symposium (International) on Combustion*, The Combustion Institute 1998, 2:2873–2880.
18. Leach, S. V., Ellzey, J. L., and Ezekoye, O. A., *Combust. Sci. Technol*., 130:247–267, (1997).
19. Williams, F. A., *Sixteenth Symposium (International) on Combustion*, 1976, pp. 1281–1294.
20. Di Blasi, C., *Combust. Sci. Technol*. 106:103–124 (1995).
21. Fatehi, M., and Kaviany, M., *Int. J. Heat Mass Transfer* 40:2607–2620 (1997).
22. Di Blasi, C., *Prog. Energy Combust. Sci*. 19:71–104 (1993).
23. Kung, H. C., *Combust. Flame* 18:185–195 (1972).
24. Dosanjh, S., Pagni, P., and Fernandez-Pello, A., *Combust. Flame* 68:131–142 (1987).

Received 23 July 1998; revised 2 June 1999; accepted 18 June 1999